2-1-1997

Optical and magneto-optical constants of MnPt3

K. W. Wierman
University of Nebraska-Lincoln

J. N. Hilfiker
University of Nebraska-Lincoln

R. F. Sabiryanov
University of Nebraska-Lincoln

Sitaram S. Jaswal
University of Nebraska-Lincoln, sjaswal1@unl.edu

Roger D. Kirby
University of Nebraska-Lincoln, rkirby1@unl.edu

See next page for additional authors

Optical and magneto-optical constants of $MnPt_3$

K. W. Wierman
Behlen Laboratory of Physics and Center for Materials Research and Analysis, University of Nebraska, Lincoln, Nebraska 68588-0113

J. N. Hilfiker
Behlen Laboratory of Physics and Center for Materials Research and Analysis, University of Nebraska, Lincoln, Nebraska 68588-0113 and Center for Microelectronic and Optical Materials Research, Department of Electrical Engineering, University of Nebraska, Lincoln, Nebraska 68588-0511

R. F. Sabiryanov, S. S. Jaswal, and R. D. Kirby
Behlen Laboratory of Physics and Center for Materials Research and Analysis, University of Nebraska, Lincoln, Nebraska 68588-0113

J. A. Woollam
Behlen Laboratory of Physics and Center for Materials Research and Analysis, University of Nebraska, Lincoln, Nebraska 68588-0113 and Center for Microelectronic and Optical Materials Research, Department of Electrical Engineering, University of Nebraska, Lincoln, Nebraska 68588-0511

(Received 19 June 1996)

Optically thick films of $MnPt_3$ were deposited on quartz using dc magnetron sputtering. The films were covered with an SiO_x protective overcoat and annealed in vacuum at 850 °C for 1 h to form the crystalline $L1_2$ (Cu_3Au) cubic structure. These films have a high degree of long-range order and are highly textured with the (111) axis along the film normal. Variable angle spectroscopic ellipsometry measurements were taken over the spectral range of 1.2–4.2 eV to determine the optical constants of both $MnPt_3$ and the SiO_x overcoat. Spectroscopic magneto-optic Kerr rotation and ellipticity measurements at near normal incidence over the spectral range of 1.4–3.6 eV were used to determine the off-diagonal dielectric tensor elements for $MnPt_3$. First-principles electronic-structure calculations were carried out for the ordered $MnPt_3$ structure and from these the dielectric tensor elements of $MnPt_3$ were calculated. The experimental and theoretical values of the diagonal components of the dielectric tensor components are in good agreement. The agreement for the off-diagonal components of the dielectric tensor is only fair. [S0163-1829(97)04205-7]

I. INTRODUCTION

The complex Kerr angle (Θ_K) fully describes the polarization state of light reflected from a magnetized surface. However, Θ_K depends on both diagonal and off-diagonal elements of the dielectric tensor in a rather complicated way, so it is often difficult to make direct associations between the calculated electronic structure and features observed in Kerr rotation and ellipticity spectra. Further, the magnitudes of the Kerr rotation and ellipticity can be greatly modified by interference effects in a multilayer structure.[1] In view of this, the connection between the macroscopic observations and microscopic theories of magneto-optic effects is perhaps best investigated by comparison of the measured and calculated dielectric (conductivity) tensor. The aim of this paper is a detailed investigation of the electronic structure of $MnPt_3$ via both experimental and theoretical studies of its complex dielectric tensor.

The stoichiometric alloy $MnPt_3$ is ferromagnetic with a Curie temperature T_C of 380 K.[2] Thin films of $MnPt_3$ have the cubic Cu_3Au ($L1_2$) structure with the Mn atoms located on the cube corners and the Pt atoms on the face-center lattice positions. With appropriate post-deposition annealing these films have a high degree of long-range order ($\eta=1.03 \pm 0.05$) and the magnetic moment is near $4\mu_B$ per formula unit ($3.6\mu_B$ on the Mn atoms and the remainder on the Pt atoms).[3–5] The films are highly textured with the (111) direction perpendicular to the film plane. Kato *et al.*[6] originally showed that films of $MnPt_3$ have a large magneto-optic response ($-1.18°$ at 1.2 eV). Since this system is highly textured and well ordered it is well suited for use in this investigation. Therefore we determine here the intrinsic dielectric tensor for $MnPt_3$ from ellipsometric and magneto-optic polar Kerr data and compare it with the dielectric tensor derived from the theoretical first-principles electronic-structure calculations.

The complex dielectric tensor (ε) for a magnetic medium with threefold or higher rotational symmetry about the z axis has the following form:

$$\varepsilon = \begin{pmatrix} \varepsilon_{xx} & \varepsilon_{xy} & 0 \\ -\varepsilon_{xy} & \varepsilon_{xx} & 0 \\ 0 & 0 & \varepsilon_{zz} \end{pmatrix}, \tag{1}$$

where in general the diagonal and off-diagonal terms are complex. Introducing the complex Voigt parameter (Q)

$$Q = \frac{i\varepsilon_{xy}}{\varepsilon_{xx}}, \tag{2}$$

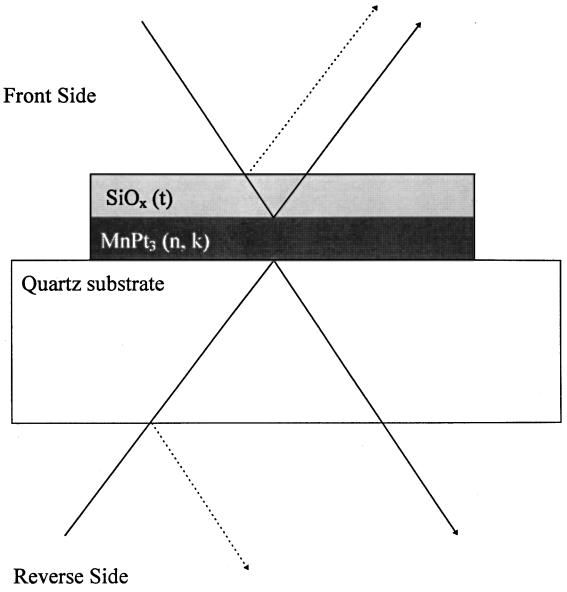

FIG. 1. Sample model used in optical/magneto-optical analysis.

and considering that ε_{zz} is not much different from ε_{xx} we obtain

$$\varepsilon=\varepsilon_{xx}\begin{pmatrix}1 & -iQ & 0\\ iQ & 1 & 0\\ 0 & 0 & 1\end{pmatrix}. \tag{3}$$

The tensor given by Eq. (3) can be diagonalized using a principal axis transformation, where the three principal axes become $x+iy$, $x-iy$, and z. Left- and right-circularly polarized light are then the eigenpolarization states corresponding to the first two principal axes. The complex indices of refraction for left- $(+)$ and right- $(-)$ circularly polarized light are in general different and expressed as

$$\tilde{n}^{\pm}=\tilde{n}(1\mp\tfrac{1}{2}\,Q) \tag{4}$$

for light propagating along the z axis. As polarized light can always be expressed as a linear combination of left- and right-circularly polarized light, a change in the polarization state of the reflected (transmitted) beam will be induced if Q is not zero. If linearly polarized light is normally incident on a magnetized sample, the plane of polarization of the reflected beam will be rotated through the Kerr angle (θ_k) and an ellipticity (η_k) will be introduced. For an optically thick magnetic film with a thick nonmagnetic dielectric overcoat the polar Kerr effect generated at nonmagnetic/magnetic interface is given by[7]

$$\theta_k+i\,\eta_k\cong -i\,\frac{\tilde{n}^{-}-\tilde{n}^{+}}{\tilde{n}^{+}\tilde{n}^{-}-\tilde{n}_n^2}\,\tilde{n}_n\cong -i\,\frac{Q\sqrt{\varepsilon_{xx}}}{\varepsilon_{xx}-\varepsilon_n}\,\sqrt{\varepsilon_n}, \tag{5}$$

where $\tilde{n}_n$ and ε_n are the complex index of refraction and dielectric constant, respectively, for the nonmagnetic medium. As can be seen from Eq. (5) the polar Kerr effect depends on the dielectric tensors of both the magnetic and nonmagnetic media in a nontrivial fashion. However, θ_k and η_k also depend on the film structure, and optical interference effects from the overcoat can play a major role in the measured Kerr effect and need be taken into account.

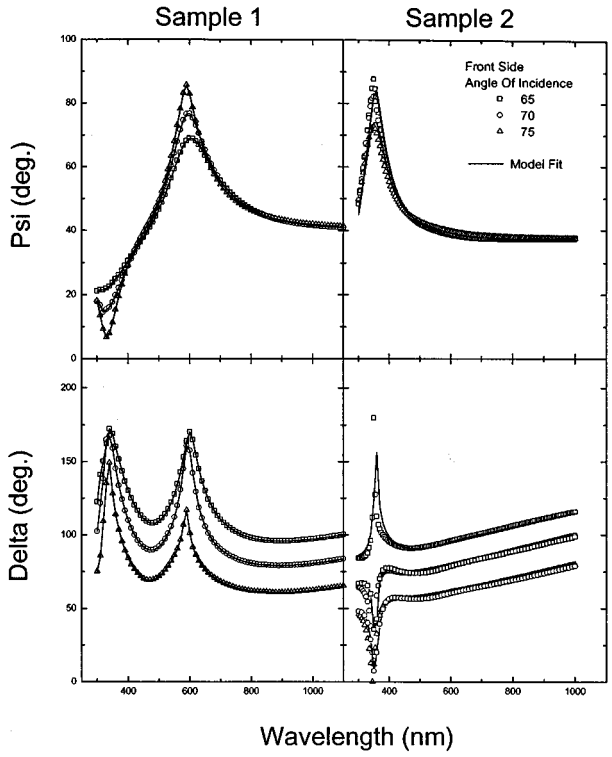

FIG. 2. Ellipsometric ψ and δ obtained from film side measurements. Data for each angle of incidence given by: 65° open square, 70° open circle, and 75° open triangle. Full line represents modeled fit for each corresponding angle of incidence.

To obtain the dielectric tensor [Eq. (3)] from experimental data we must solve Maxwell's equations for our thin-film structure. The formalism for this procedure is outlined in detail in Refs. 8, 9 and 10. The natural solutions to the wave equation can be expressed in terms of the indices of refraction for left- and right-circularly polarized light as given by Eq. (4). By utilizing variable angle spectroscopic ellipsometry and magneto-optic Kerr effect measurement and analysis techniques we can obtain the intrinsic indices of refraction $(\tilde{n}=n+ik)$ and magneto-optic Voigt parameter $(Q=Q'+iQ'')$ for $MnPt_3$. These parameters can then be related to the dielectric tensor by using Eq. (2) and the following relation:

$$\varepsilon_{xx}=(n^2-k^2)+i2nk. \tag{6}$$

II. DIELECTRIC TENSOR CALCULATIONS

The complex conductivity tensor (σ) for interband transitions in the random-phase approximation without allowance for the local-field effects is given by[11]

$$\sigma_{\alpha\beta}(\omega)=\frac{1}{\pi}\int d\omega' I(\omega')\left(\frac{1}{\omega-\omega'+i/\tau}+\frac{1}{\omega+\omega'+i/\tau}\right), \tag{7}$$

where τ is the relaxation time and the expression for $I(\omega)$ is given below,

TABLE I. Sample parameters.

	SiO_x layer thickness (t in nm)		$MnPt_3$ (t in nm)
Samples	Nominal	Fitted	Nominal
1	100	98.7	100
2	50	49.9	100

$$I(\omega)=\frac{\pi e^2}{2\omega}\sum_{\mathbf{k}\lambda\neq\lambda'}\delta(\hbar\omega-E_{\lambda\lambda'}(\mathbf{k}))\{\theta(E_\lambda(\mathbf{k})-E_F)-\theta(E_{\lambda'}(\mathbf{k})-E_F)\}[j_\alpha^{\lambda\lambda'}(\mathbf{k})j_\beta^{\lambda'\lambda}(\mathbf{k})] \tag{8}$$

Here, E_F is the Fermi energy, and $E_{\lambda\lambda'}(\mathbf{k})$ is the difference in the energies of the one-electron states $|\mathbf{k}\lambda\rangle$ and $|\mathbf{k}\lambda'\rangle$. The Fermi function has been replaced with the step function θ and the matrix elements of the current density operator are given by

$$j_\alpha^{\lambda\lambda'}(\mathbf{k})=\langle\mathbf{k}\lambda|\nabla_\alpha|\mathbf{k}\lambda'\rangle. \tag{9}$$

We use the linear-muffin-tin-orbital (LMTO) method[12] in the near-orthogonal representation to perform spin-polarized self-consistent electronic-structure calculations with the scalar-relativistic and spin-orbit correction terms included in the Hamiltonian. The local-density LMTO calculations are based on the atomic-sphere approximation corrected to first order by the combined correction term.[13] The details of the calculation of the matrix elements of the current density operator in terms of the LMTO method are given in Ref. 13. The linear tetrahedron method is used to calculate the real and imaginary parts of σ simultaneously, thereby avoiding the numerical errors that can arise in a Kramers-Kronig transformation.[14,15] The dielectric tensor (ε) can then be related to the conductivity tensor by

$$\varepsilon_{ij}=\delta_{ij}+\frac{i4\pi}{\omega}\sigma_{ij}+\chi_{\mathrm{FC}}(\omega)\delta_{ij}, \tag{10}$$

where the intraband contribution due to the free carriers (χ_{FC}) to the diagonal component of the dielectric tensor is given by the Drude model

$$\chi_{\mathrm{FC}}(\omega)=-\frac{\omega_p^2}{\omega(\omega+i\gamma)}. \tag{11}$$

Here ω_p is the plasma frequency and γ is the collision frequency. In the single-frequency approach ω_p is given by[16]

$$\omega_p^2=\frac{4\pi e^2}{\Omega}\sum_{\mathbf{k}\lambda}|\mathbf{V}_{\mathbf{k}\lambda}|^2\delta(E_{\mathbf{k}\lambda}-E_F), \tag{12}$$

where Ω is the volume of the primitive cell and

$$\mathbf{V}_{\mathbf{k}\lambda}=\langle\mathbf{k}\lambda|\nabla|\mathbf{k}\lambda\rangle \tag{13}$$

is the mean velocity of an electron in state $|\mathbf{k}\lambda\rangle$.

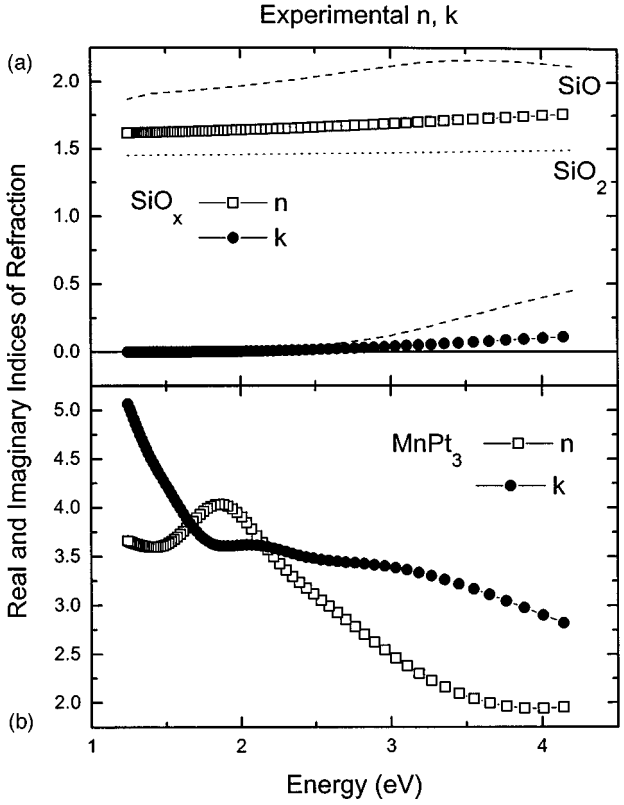

FIG. 3. Indices of refraction for (a) SiO_x protective overcoat, (b) $MnPt_3$. Dashed lines represent indices of refraction for SiO and SiO_2 obtained from Ref. 22.

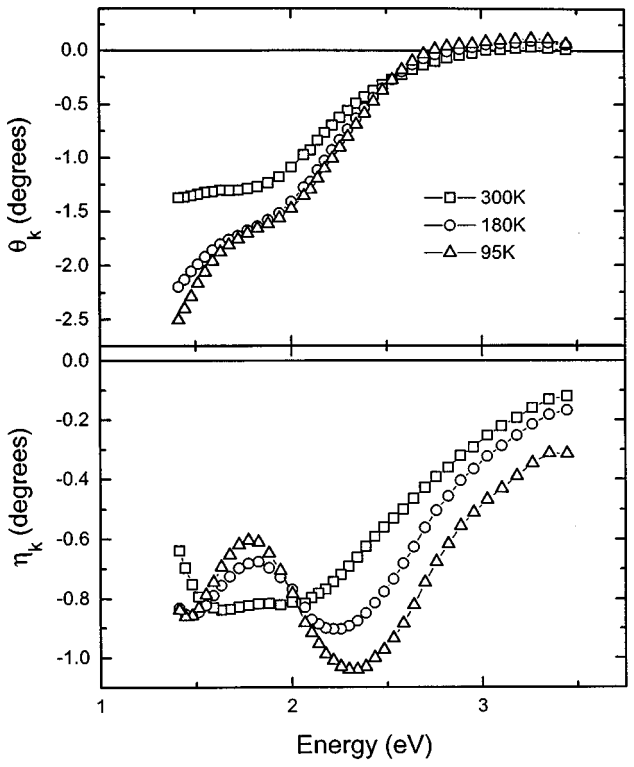

FIG. 4. Kerr rotation (θ_k) and ellipticity (η_k) of $MnPt_3$ from film side measurements. Different temperatures are represented by 300 K open square, 180 K open circle, and 95 K open triangle.

III. EXPERIMENTAL PROCEDURES AND DATA ANALYSIS

A. Sample preparation

Samples of optically thick $MnPt_3$ thin films on quartz substrates were prepared by dc magnetron sputtering and covered with either a 50 or 100 nm SiO_x protective overcoat. The samples were annealed in vacuum at 850 °C for 1 h to form the crystalline $L1_2$ (Cu_3Au) cubic structure. The crystalline structure was confirmed by x-ray diffraction. X-ray fluorescence measurements on the as-deposited films showed they were close to nominal compositions ($\pm 2\%$). A Curie temperature of 375 ± 5 K was measured for each sample. To further reduce the number of adjustable parameters a sample consisting of a 300 nm thick SiO_x layer deposited on a Si (100) substrate was made. Ellipsometric measurements were taken at three angles (65°, 70°, and 75°) near the pseudo-Brewster angle, over the spectral range from 1.2–4.2 eV. This maximizes the tradeoff between the magnitude of the ellipsometric parameters and light intensity.

The indices of refraction for the SiO_x layer were determined by analyzing the ellipsometric data from the SiO_x/Si sample. A Cauchy dispersion model was used to fit the ellipsometric data by varying the indices of refraction (n,k) and thickness (t) of the SiO_x layer. The indices of refraction of the silicon substrate were taken from Ref. 22.

B. Ellipsometry

In general the amplitudes and phases of the *s* and *p* polarization components of the incident light are altered differently by a sample upon reflection or transmission. Variable angle ellipsometry can be used to measure this change in the polarization state over a wide range of wavelengths and angles of incidence. For reflection the measurable ellipsometric parameters Ψ and Δ at some nonnormal angle of incidence are defined by

$$\tan\psi e^{i\nabla} \equiv \frac{\tilde{r}_p}{\tilde{r}_s}, \tag{14}$$

where r_s and r_p are the Fresnel reflection coefficients derived from solving Maxwell's equations of electrodynamics at the interface between two optically distinguishable media and *s* and *p* indicate the electric vector perpendicular and parallel to the plane of incidence, respectively. A convenient formalism embodying the solutions to Maxwell's equations uses a general 4×4 matrix whose form relates the propagation of the electric and magnetic field through the layer. This 4×4 matrix, defined as the characteristic matrix, relates the continuous tangential components of the electromagnetic field at any two planes in the system and contains the imposed boundary conditions and material parameters.[17] The characteristic matrix of the multilayer stack is then simply the product of the characteristic matrix for each individual layer and substrate in the proper order.[18] This procedure allows the development of an optical/magneto-optical sample model that accounts for all interface and interference optical effects.

The Fresnel coefficients are functions of the angle of incidence, the complex indices of refraction of the sample, and the layer thickness. It is not feasible to directly solve the nonlinear equations, Eq. (14), for the unknown indices of refraction (n,k) and layer thicknesses from the measured ellipsometric data. Instead the sample parameters are determined by a least-squares fitting to the observed ellipsometric parameters ψ and Δ as follows. Predicted values for ψ and Δ over the spectral range and angle of incidence are obtained using the sample model as described above. A comparison between the predicted and experimental ψ and Δ is made using a mean-squared-error (MSE) formula

$$\mathrm{MSE} = \left[\frac{1}{2N-M} \sum_{i=1}^{N} \frac{(\omega^C - \omega^M)^2}{\xi_{\psi_i}^2} + \frac{(\Delta^C - \Delta^M)^2}{\xi_{\Delta_i}^2} \right]^2, \tag{15}$$

where C and M signify the calculated and measured parameters, respectively, N is the number of (ψ,Δ) pairs, M is the number of variable parameters in the model, and ξ_i are the standard deviations of the measurements.[19] The Levenberg-Marquardt multivariate regression algorithm is used to fit the model to experimental data by varying the material parameters in order to minimize the difference between model and experiment. To determine a set of parameters that provide a good fit to the experimental data the correlation between variable parameters must be minimized. This can be accomplished by analyzing several samples prepared under similar conditions, but with different physical structures (i.e., the determined optical constants of the materials are consistent while the layer thicknesses are changed).

A variable angle spectroscopic ellipsometric system based on the rotating analyzer method was utilized to acquire the experimental ψ and Δ data over the 1.2–4.2 eV range (J. A. Woollam Co., VASE®).[20] The ψ and Δ data thus obtained were then analyzed using Levenberg-Marquardt algorithm described earlier.

Once the indices of refraction and layer thicknesses for SiO_x and $MnPt_3$ are determined, it is then possible to determine the Voigt parameter from the experimental θ_k and η_k. The magneto-optic data were acquired using a home-built instrument based on a photoelastic modulator (PEM).[21] The PEM is a compensator with a time-varying phase retardation and is used to rapidly oscillate, at 50 kHz, the polarization state of the incident light. The accuracy of the system is $\pm 0.005°$ over the spectral range. The same sample model used to analyze the ellipsometric data is used here to generate a predicted experimental θ_k and η_k. The same procedure of using MSE and the Lavenberg-Marquardt algorithm as described above is then applied to determine the intrinsic magneto-optic Voigt parameter.

IV. RESULTS AND DISCUSSION

Figure 1 shows the layered structure for one $MnPt_3$ film sample. The ellipsometry measurements were then interpreted in terms of this model. The ellipsometry measurements were made with light incident from both sides of the film. In the case of light incident from the quartz substrate side, multiple reflections were treated incoherently. For measurements with the light incident from the SiO_x side, the values of n and k determined for SiO_x/Si were used as fixed constants. The n and k values for the quartz substrate were obtained from Ref. 22. The additional information provided by reverse side measurements has been shown to reduce the

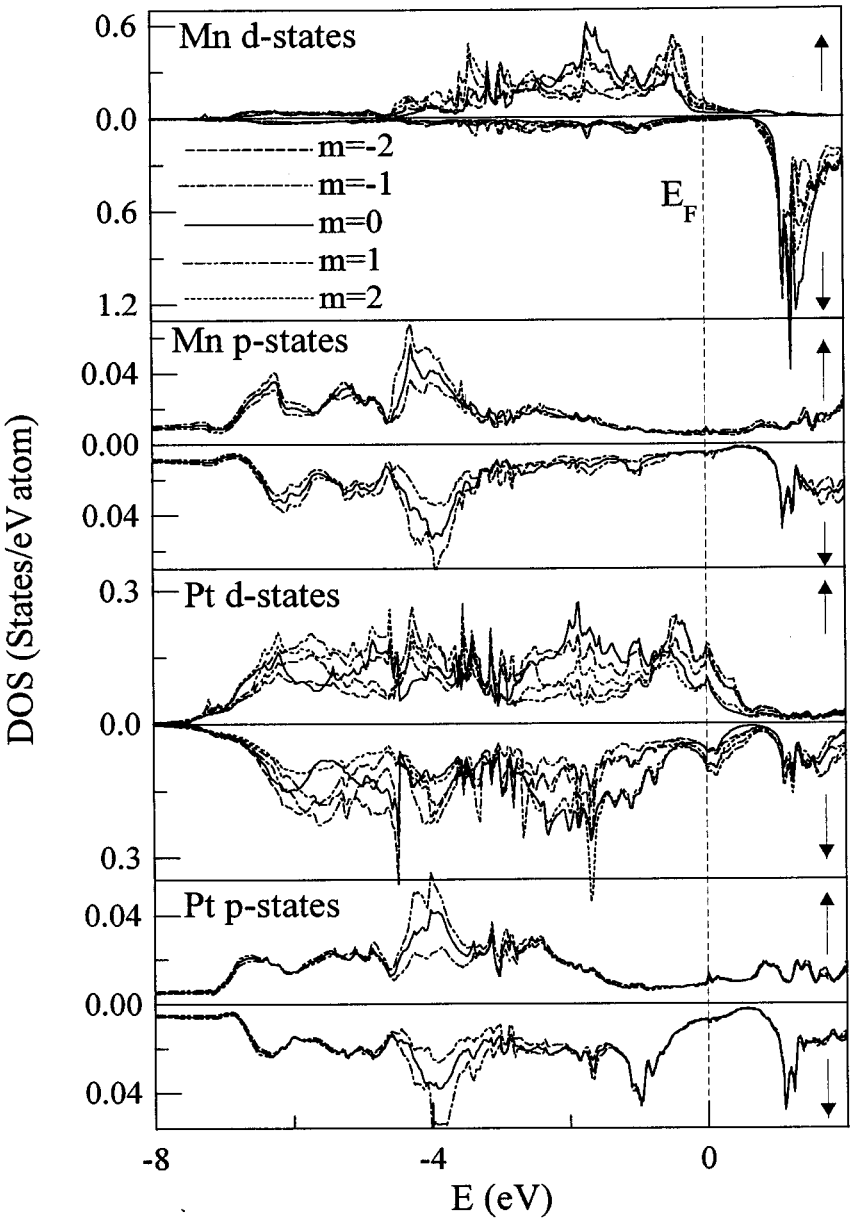

FIG. 5. Spin-polarized Mn and Pt orbital-magnetic-quantum number (m) projected densities of states of $MnPt_3$.

correlation between variable parameters.[23] The variable parameters that are fitted are the n and k of the $MnPt_3$ layer and the thickness of the SiO_x layer.

Figure 2 shows the model fit to ellipsometric data of ψ and Δ for samples 1 and 2, with the SiO_x layer fitted results given in Table I. For both samples ellipsometric data fit well to the derived optical constants. Figure 3 gives the experimentally derived n and k for SiO_x and $MnPt_3$. The real part of the index of refraction for $MnPt_3$ has a broad peak at 1.8 eV which is quite different than what is seen in bulk Pt and Mn where a general decrease in n and k with decreasing photon energy is shown in Ref. 22. Figure 4 shows the Kerr rotation data at three different temperatures (95, 180, and 300 K). There is a general monatomic decrease in the magnitudes of θ_k and η_k with increasing temperature, and the peak in η_k between 1.5–2.0 eV decreases in magnitude with increasing temperature. This spectral region corresponds to the broad peak in n at 1.8 eV.

To present a qualitative understanding of the electronic states involved in determining the magneto-optic properties of $MnPt_3$, the orbital magnetic quantum number (m) projected densities of states (DOS) for the spin-polarized p and d states of Mn and Pt are plotted in Fig. 5. These are the states that primarily determine the Kerr rotation in this system. It is interesting to note that Mn DOS shows an almost half-metallic behavior in the spin-down state. Figure 5 also shows that the unoccupied states consist primarily of a fairly localized Mn minority band around 1.0 eV above the Fermi energy (E_F) and a corresponding Pt band in the same region induced by the Mn band through hybridization. Thus the Kerr rotation is determined mainly by the transitions from the minority occupied states to the above-mentioned unoccupied bands. A system has nonzero Kerr rotation if the dipole matrix elements for the left-circularly-polarized light ($\Delta m = -1$) are different from those of the right-circularly-polarized light ($\Delta m = +1$). This is possible when the projected DOS

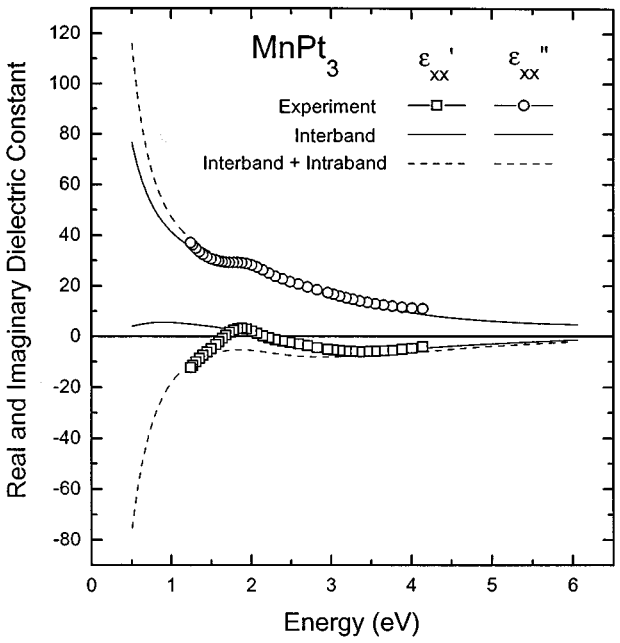

FIG. 6. Real and imaginary parts of ε_{xx} of $MnPt_3$. Experimentally derived values are given by open circles and squares, respectively. Solid line gives the calculated results with interband contributions only while the dashed line includes both interband and intraband contributions, ($\hbar/\tau$=0.5 eV, $\hbar\gamma$=0.3 eV, and $\hbar\omega_p$=5 eV).

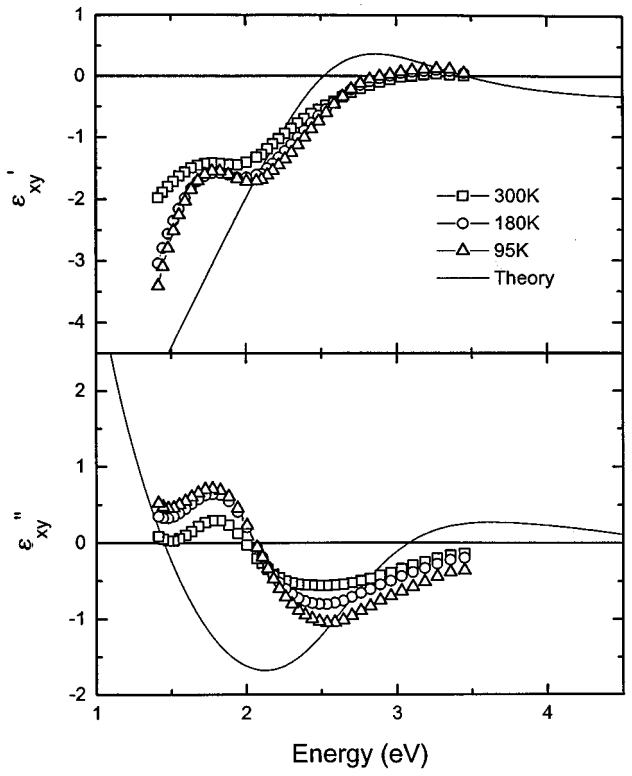

FIG. 7. Real and imaginary parts of ε_{xy} of $MnPt_3$. Experimentally derived values for each temperatures are represented by 300 K open square, 180 K open circle, and 95 K open triangle. Solid line gives the calculated results with interband contributions only.

for $+m$ is not equal to that of $-m$ for a given orbital number l in a ferromagnetic system. This condition is satisfied in $MnPt_3$ as can be seen from the m-projected DOS in Fig. 5.

The real and imaginary parts of the diagonal component of the dielectric tensor from experiment and theory are compared in Fig. 6. The calculated results based on the inter- and intraband ($\hbar/\tau$=0.5 eV, $\hbar\gamma$=0.3 eV, and $\hbar\omega_p$=5 eV) contributions are in good agreement with the experimental data. We will comment later on the structure in the experimental data around 1.8 eV. Figure 7 shows the real and imaginary parts of the off-diagonal component of the dielectric tensor. The agreement is only fair in the sense that theory predicts only the general trends in the experimental data. The theoretical results are shifted down in energy with respect to the experimental data by approximately 0.5 eV, a result similar to that found by Openeer *et al.*[24] Openeer *et al.* also found that this shift is not sensitive to the scaling of spin-orbit interactions. The shift may be due to the failure of the local-density theory (LDA) to correctly predict the position of the fairly localized unoccupied Mn band. The LDA underestimates the position of similarly localized unoccupied $4f$ bands in rare earths and $3d$ bands in insulating transition-metal compounds (oxides, sulfides).[25,26] This shortcoming of LDA is not reflected in the diagonal tensor components (Fig. 5) because of their weak dependence on the energy in the interband transition region. The off-diagonal components are much more sensitive to the details of the electronic structure than the diagonal components because the former depend on the difference while the latter on the sum of the dipole matrix elements of the left- and right-circularly-polarized light. Regarding the absence of the structure in the theoretical dielectric tensor around 1.8 eV, the Drude model seems to be overestimating the intraband contribution as one goes to higher energies. One can see from Fig. 6 that an upward shift in energy of the theoretical curves by approximately 0.5 eV and the above-mentioned modification of the intraband contribution will lead to a good agreement between the general shape of the theoretical and experimental curves.

V. CONCLUSIONS

The complete complex dielectric tensor for $MnPt_3$ has been obtained by using a combination of ellipsometric and magneto-optic techniques. The dielectric diagonal components agree extremely well with theoretical calculations. The agreement between the experiment and theory for the off-diagonal component of the dielectric tensor is only fair. This may be due to the limitations of the local-density approximation in electronic-structure calculations and the Drude model for the intraband contributions. We plan to go beyond the local-density approximation and find ways to include the temperature effects on the magneto-optical properties in the future.

ACKNOWLEDGMENTS

The authors are grateful to Dan Thompson for many helpful discussions. The research described in this publication was made possible by Grant No. OSR-9255225 from the National Science Foundation, and support from the Center of Material Research and Analysis is appreciated.

[1] D. O. Smith, Opt. Acta **12**, 193 (1965).
[2] M. Auwärter and A. Kussman, Anal. Phys. **7**, 90 (1967).
[3] K. W. Wierman and R. D. Kirby, J. Magn. Magn. Mater. **154**, 12 (1996).
[4] S. J. Pickart and R. Nathans, J. Appl. Phys. **33**, 1336 (1962).
[5] B. Antonini, F. Lucari, P. Menzinger, and A. Paletti, Phys. Rev. **187**, 611 (1969).
[6] T. Kato, H. Kikuzuwa, S. Iwata, S. Tsunashima, and S. Uchiyama, J. Magn. Magn. Mater. **140–141**, 713 (1995).
[7] A. V. Sokolov, *Optical Properties of Metals* (Elsevier, New York, 1967).
[8] W. A. McGahan and J. A. Woollam, Appl. Phys. Commun. **9**, 1 (1989).
[9] P. He, W. A. McGahan, and J. A. Woollam, Proc. SPIE **1499**, 401 (1991).
[10] W. A. McGahan, P. He, and J. A. Woollam, Appl. Phys. Commun. **11**, 375 (1992).
[11] C. S. Wang and D. J. Callaway, Phys. Rev. B **9**, 4897 (1974).
[12] O. K. Andersen, Phys. Rev. B **12**, 3060 (1975).
[13] Y. A. Uspenskii and S. V. Khalilov, Sov. Phys. JETP **68**, 588 (1989); Y. A. Uspenskii, F. G. Maksimov, S. N. Rashkeev, and I. I. Mazin, Z. Phys. B **53**, 263 (1983).
[14] R. F. Sabiryanov and S. S. Jaswal, Phys. Rev. B **53**, 313 (1996).
[15] P. Lambin and J. P. Vigneron, Phys. Rev. B **29**, 3430 (1984).
[16] I. I. Mazin, Y. G. Maksimov, S. N. Rashkeyev, and Y. A. Uspenskii, *Metal Optics and Superconductivity*, edited by A. I. Golovashkin (Nova Science, New York, 1989), p. 1.
[17] D. O. Smith, Opt. Acta **12**, 13 (1965).
[18] P. H. Lissberger, Rep. Prog. Phys. **33**, 197 (1970).
[19] *Guide to using WVASE32* (Woollam, Lincoln, 1995), pp. 6–15.
[20] *Guide to using WVASE32* (Ref. 19), pp. 31–32.
[21] U. Rossow and W. Richter, in *Optical Characterization of Epitaxial Semiconductor Layers*, edited by Günther Bauer and Wolfgang Richter (Springer-Verlag, Berlin, 1996), pp. 68–85.
[22] *Handbook of Optical Constants of Solids*, edited by E. Palik (Academic, New York, 1985).
[23] B. D. Johs, W. A. McGahan, and J. A. Woollam, Thin Solid Films **253**, 25 (1994).
[24] P. M. Openeer, V. N. Antonov, T. Kraft, H. Eshrig, A. N. Yareska, and A. Y. Pervov, Solid State Commun. **94**, 255 (1995).
[25] B. N. Harmon, V. P. Antropov, A. I. Liechtenstein, I. V. Solovyev, and V. I. Anisimov, J. Phys. Chem. Solids **56**, 1521 (1995).
[26] A. Svane and O. Gunnarsson, Phys. Rev. Lett. **65**, 1148 (1990).